Chapter 15

Mosaicing

Fréderic Gueth

Max Planck Institute für Radioastronomie, Auf dem Hügel 69, D-5300 Bonn

15.1 Introduction

The dirty map F resulting from a normal, single-field interferometric observation can be described by the equation:

$$F = D * (B \times I) + N \tag{15.1}$$

where D is the dirty beam, B the antenna primary beam, I the sky brightness distribution, and N a noise distribution[1]. The interferometer is only sensitive to the product of the sky brightness distribution by the rapidly decreasing function B. As the noise distribution N is not affected by B, any attempt to correct for the primary beam attenuation (i.e. divide the clean map by B) results in a strongly increasing noise. Hence, the primary beam attenuation limits the size of the region it is possible to map with an interferometer.

Due to the coupling between the receiver horn and the primary mirror of the antennas (see lecture by A. Greve), the primary beam B is, to a good approximation, a gaussian. Its FWHM (proportional to the ratio of the wavelength λ to the antenna diameter $\mathcal{D}$) can therefore be used to define a "field of view". Table 15.1 gives the resulting values for the Plateau de Bure interferometer, for different frequencies. To map regions more extended than the primary beam width, it is necessary to observe a *mosaic* of several adjacent fields. Clearly, due to the gaussian-shape of the primary beam attenuation, these fields have to strongly overlap to ensure a roughly uniform sensitivity over the whole mapped region.

A further complication arises from the lack of the short-spacings information in the interferometer data set. Due to their diameter, the antennas cannot be put too close to each other, which results in a minimal measured baseline (24 m at the Plateau de Bure). Even if projection effects reduce the effective baselines, a central "hole" in the data distribution in the uv plane cannot be avoided. As a consequence, the extended structures (whose visibilities are confined in a small region in the uv plane) are filtered

[1] In the following, we will assume an uniform noise rms, i.e. we do not take into account variation of the noise introduced by the imaging process (see lecture by S. Guilloteau).

Frequency (GHz)	Wavelength (mm)	Field of View ($''$)	Largest structure ($''$)
85	3.5	58	36
100	3.0	50	31
115	2.6	43	27
215	1.4	23	14
230	1.3	21.5	13
245	1.2	20	12

Table 15.1: Field of view of the Plateau de Bure interferometer: the 15 m dishes have a gaussian illumination, which yields a nearly gaussian primary beam. The two groups of frequencies correspond to the two receivers that are currently available. The last column gives *rough estimates* of the size of the largest structure which can be observed.

out. The largest structure it is possible to map with a single-field interferometric observation is thus even smaller than the field of view, and can be very roughly estimated by the ratio of the wavelength to the minimal baseline (Table 15.1). In the framework of mosaic observations, the short-spacings problem has however to be thought in slightly different terms, because it introduces now artifacts on an intermediate scale (see Sec. 15.5) but also because it can, at least in theory, be partially solved (Sec. 15.2).

15.2 Image formation in a mosaic

Some important mosaic properties can be understood by analyzing the combination of the data directly in the uv plane. This analysis was first proposed by [Ekers & Rots 1979]. The reader is also referred to [Cornwell 1989]. We consider a source whose brightness distribution is $I(x, y)$ (where x and m are two angular coordinates), and whose "true" visibility (i.e. the Fourier transform of I) is noted V. A two-antenna interferometer, whose primary beam is $B(x, y)$, will measure a visibility at a point (u, v) which may be written as:

$$V_{\rm mes}(u,v) = \iint_{-\infty}^{+\infty} B(x,y)\, I(x,y)\, {\rm e}^{-2i\pi(ux+vy)}\, dx\, dy \tag{15.2}$$

For an observation with a phase center in $(x = 0, m = 0)$ but with a pointing center in (x_p, y_p), the measured visibility (whose dependence on (x_p, y_p) is here explicitly indicated) is now:

$$V_{\rm mes}(u,v,x_p,y_p) = \iint_{-\infty}^{+\infty} B(x-x_p, y-y_p)\, I(x,y)\, {\rm e}^{-2i\pi(ux+vy)}\, dx\, dy \tag{15.3}$$

For further use, this last relation can also be rewritten, using the symmetry properties of the primary beam B:

$$V_{\rm mes}(u,v,x_p,y_p) = B(x_p,y_p) * \mathcal{F}(u,v,x_p,y_p) \tag{15.4}$$

where $*$ denotes a convolution product and the function $\mathcal{F}$ is defined as:

$$\mathcal{F}(u,v,x_p,y_p) = I(x_p,y_p)\, {\rm e}^{-2i\pi(ux_p+vy_p)} \tag{15.5}$$

Now, imagine an ideal "on-the-fly" mosaic experiment: for a given, fixed (u, v) point, the pointing center is continuously modified, and the variation of the visibility with $(x_p,\, y_p)$ can thus be monitored. Then, the Fourier transform of $V_{\rm mes}$ with respect to (x_p, y_p) gives (from equation 15.4):

$$[{\rm FT_p}(V_{\rm mes})]\,(u_p,v_p) = T(u_p,v_p)\, V(u+u_p, v+v_p) \tag{15.6}$$

where:

- $\mathrm{FT_p}$ denotes the Fourier transform with respect to (x_p, y_p) and (u_p, v_p) are the conjugate variables to (x_p, y_p).
- $[\mathrm{FT_p}(V_{\mathrm{mes}})]\,(u_p, v_p)$ is the Fourier transform of the observations.
- $T(u_p, v_p)$ is the Fourier transform of the primary beam $B(x_p, y_p)$. T is thus the transfer function of each antenna. For a dish of diameter $\mathcal{D}$, $T(u_p, v_p) = 0$ if $\sqrt{u_p^2 + v_p^2} > \mathcal{D}/\lambda$.
- $V(u + u_p, v + v_p)$ is the Fourier transform of $\mathcal{F}(u, v, x_p, y_p)$ with respect to (x_p, y_p). Indeed, $\mathcal{F}$ is the product of the sky brightness distribution (whose Fourier transform is V) by a phase term, and its own Fourier transform is thus simply V taken at a shifted point.

For $\sqrt{u_p^2 + v_p^2} < \mathcal{D}/\lambda$, we can thus derive:

$$V(u + u_p, v + v_p) = \frac{[\mathrm{FT_p}(V_{\mathrm{mes}})]\,(u_p, v_p)}{T(u_p, v_p)} \tag{15.7}$$

This relation illustrates an important property of the experiment we have considered. The observations were performed at a given (u, v) point but with a varying pointing center. Equation 15.7 shows that is possible to derive from this data set the visibility $V(u + u_p, v + v_p)$ at all (u_p, v_p) which verify $(u_p^2 + v_p^2)^{1/2} < \mathcal{D}/\lambda$. In other terms, the measurements have been done at (u, v) but the redundancy of the observations allows to compute (through a Fourier transform and a division by the antenna transfer function) the source visibility at all the points of a disk of radius $\mathcal{D}/\lambda$, centered in (u, v).

Interpretation

In very pictorial terms, one can say that the adjacent pointing reinforce each other and thereby yield a estimate of the source visibility at unmeasured points. Note however that the resulting image quality is not going to be drastically increased: more information can be extracted from the data, but a much more extended region has now to be mapped[2]. The redundancy of the observations has only allowed to rearrange the information in the uv-plane. This is nevertheless extremely important, as e.g. it allows the estimate part of the missing short-spacings (see below).

How is it possible to recover unmeasured spacings in the uv-plane? It is actually obvious that two antennas of diameter $\mathcal{D}$, separated by a distance $\mathcal{B}$, are sensitive to all the baselines ranging from $\mathcal{B} - \mathcal{D}$ to $\mathcal{B} + \mathcal{D}$. The measured visibility is therefore an average of all these baselines: V_{mes} is actually the convolution of the "true" visibility by the transfer function of the antennas. This is shown by the Fourier transform of equation 15.2, which yields: $V_{\mathrm{mes}} = T * V$. Now, if the pointing center and the phase center differ, a phase gradient is introduced across the antenna apertures, which means that the transfer function is affected by a phase term. Indeed, the Fourier transform of equation 15.3 yields:

$$V_{\mathrm{mes}}(u, v) = \left[T(u, v)\,\mathrm{e}^{-2i\pi(ux_p + vy_p)}\right] * V(u, v) \tag{15.8}$$

Hence, the measured visibilities are (still) a linear combination of the "true" visibilities. Measurements performed in various directions (x_p, y_p) give many such linear combinations. One can thus expect to derive from this linear system the initial visibilities, in the baseline range from $\mathcal{B} - \mathcal{D}$ to $\mathcal{B} + \mathcal{D}$. Equation 15.7 just shows that a Fourier transform allows to do that.

Field spacing in a mosaic

In the above analysis, a continuous drift of the pointing center was considered. However, the same results can be reached in the case of a limited number of pointings, provided that classical sampling theorems are fulfilled. We want to compute the visibility in a finite domain, which extends up to $\pm\mathcal{D}/\lambda$ around the nominal center, and therefore the pointing centers have to be separated by $\lambda/2\mathcal{D}$ (see [Cornwell 1988]).

[2] We have considered observations of different directions, performed with the same uv-coverage. The analysis presented here shows that such an experiment is somehow equivalent to the observation of the whole source, but with a different, more complete uv-coverage.

In practice, the (gaussian) transfer function of the millimeter dishes drops so fast that one can use without consequences a slightly broader, more convenient sampling, equal to half the primary beam width (i.e. $1.2\,\lambda/2\mathcal{D}$).

Mosaics and short-spacings

As with any other measured point in the uv plane, it is possible to derive visibilities in a small region (a disk of diameter $\mathcal{D}/\lambda$) around the shortest measured baseline. This is the meaning of the statement that mosaics can recover part of the short-spacings information: a mosaic will include (u,v) points corresponding to the shortest baseline minus $\mathcal{D}/\lambda$.

In practice, however, things are more complex. First, we have to deal with noisy data. As a consequence, it is not possible to expect a gain of $\mathcal{D}/\lambda$: the transfer function T which is used in equation 15.7 is strongly decreasing, and therefore signal-to-noise ratio limits the gain in the uv plane to a smaller value, typically $\mathcal{D}/2\lambda$ ([Cornwell 1988]). This is still a very useful gain: for the Plateau de Bure interferometer, this corresponds to a distance in the uv plane of 7.5 m, while the shortest (unprojected) baseline is 24 m. Secondly, the analysis described above would be rather difficult to implement with real observations. Instead, one prefers to combine the observed fields to directly reconstruct the sky brightness distribution. The resulting image should include the information arising from the redundancy of the adjacent fields, among them part of the short-spacings. However, the complexity of the reconstruction and deconvolution algorithms that have to be used precludes any detailed mathematical analysis of the structures of the maps. For instance, the (unavoidable) deconvolution of the image can also be interpreted as an interpolation process in the uv plane (see [Schwarz 1978]) for the case of the CLEAN algorithm) and its effects can thus hardly be distinguish from the intrinsic determination of unmeasured visibilities that occur when mosaicing.

15.3 Mosaicing in practice

Observation and calibration

The observation of a mosaic with the Plateau de Bure interferometer and the calibration of the data do not present any specific difficulties. We just mention here a few practical remarks:

- As shown in the previous paragraph, the optimal spacing between adjacent fields is half the primary beam width. Larger separations can be used (e.g. to map larger field of view in the same amount of time) but the image reconstruction is not optimal in that case. Note that if the two receivers are used simultaneously, the field spacing has to be adapted to one of the frequencies, which results in an over- or undersampling for the other one.

- Even if this is not formally required by the reconstruction and deconvolution algorithm described in the following section, it seems quite important to ensure similar observing conditions for all the pointing centers. Ideally, one would want the same noise level in each field, so that the noise in the final image is uniform, and the same uv coverage, to avoid strong discrepancies (in terms of angular resolution and image artifacts) between the different parts of the mosaic. To handle these constraints in practice, the fields are observed in a loop, each one during a few minutes (similarly to snapshot observations of several sources): hence, atmospheric conditions and uv coverage are similar for all the fields.

- In most cases, a mosaic will not be observed during an amount of time significantly larger than normal projects. As the observing time is shared between the different pointing centers, the sensitivity of each individual field is thus smaller than what would have been achieved with normal single-field observations. Note however that the sensitivity is further increased in the mosaic, thanks to the strong overlap between the adjacent fields (see Fig. 15.1).

- The maximal number of fields it is possible to observe in a mosaic is limited by observational constraints. The fields are observed in a loop, one after the other, and to get a reasonable uv

coverage within one transit, only a limited number of fields can be observed. With the Plateau de Bure interferometer, the limit seems to be around 15 fields. Mosaicing even more fields would probably require some other approach (e.g. mosaic of several mosaics). Finally, a potential practical limitation is the disk and memory sizes of the computers, as mosaicing requires to handle very large images.

- The calibration of a mosaic is strictly identical with any other observation performed with the Plateau de Bure interferometer, as only the observations of the calibrators are used. At the end of the calibration process, a *uv* table and then a dirty map are computed for each pointing center.

Mosaic reconstruction

The point is now to reconstruct a mosaic from the observations of each field, in an optimal way in terms of signal-to-noise ratio. Just forget for the time being the effects of the convolution by the dirty beam. Each field i can thus be written: $F_i = B_i \times I + N_i$, where B_i is the primary beam of the interferometer, centered in a different direction for each observation i, and N_i is the corresponding noise distribution. In practice, the same phase center (i.e. the same coordinate system) is used for all the fields. We are thus in the classical framework of several observations of the same unknown quantity I, each one being affected by a weighting factor B_i. The best estimate of I, in the least-square sense, is thus given by:

$$\widetilde{I} = \frac{\sum_i \frac{B_i}{\sigma_i^2} F_i}{\sum_i \frac{B_i^2}{\sigma_i^2}} \tag{15.9}$$

where the sum includes all the observed fields and σ_i is the rms of the noise distribution N_i. (Note that in Eq.15.9 as well as in the following equations, σ_i is a number while other letters denote two-dimensional distributions).

Linear vs. non-linear mosaics

The problem which remains to be address is the deconvolution of the mosaic. This is actually the main difficulty of mosaic interferometric observations. Two different approaches have been proposed (e.g. [Cornwell 1993]):

- *Linear mosaicing:* each field is deconvolved using classical technics, and a mosaic is reconstructed afterwards with the clean images, according to equation 15.9.

- *Non-linear mosaicing:* a joint deconvolution of all the fields is performed, i.e. the reconstruction and the deconvolution of the mosaic are done simultaneously.

The deconvolution algorithms are highly non-linear, and the two methods are therefore not equivalent. The first one is straightforward to implement, but the non-linear mosaicing algorithms give much better results. Indeed, the combination of the adjacent fields in a mosaic allows to estimate visibilities which were not observed (see previous paragraph), it allows to remove sidelobes in the whole mapped area, and it increases the sensitivity in the (large) overlapping regions: these effects make the deconvolution much more efficient.

Non-linear deconvolution methods based on the `MEM` algorithm have been proposed by [Cornwell 1988]) and [Sault et al 1996]. As CLEAN deconvolutions are usually applied on Plateau de Bure data, a CLEAN-based method adapted to the case of the mosaics has been developed. The initial idea was proposed by F. Viallefond (DEMIRM, Paris) and S. Guilloteau (IRAM), and the algorithm is now implemented in the MAPPING software.

15.4 A CLEAN-based algorithm for mosaic deconvolution

The dirty mosaic

The dirty maps of each field i are computed with the same phase center (i.e. the same coordinate system) and can therefore be written:

$$F_i = D_i * (B_i \times I) + N_i \tag{15.10}$$

Note that the dirty beams D_i are *a priori* different for each pointing center, because the uv coverages, even if similar, are slightly different. The dirty mosaic J can then be constructed according to equation 15.9:

$$J = \frac{\sum_i \frac{B_i}{\sigma_i^2} F_i}{\sum_i \frac{B_i^2}{\sigma_i^2}} = \frac{\sum_i B_i\, \sigma_i^{-2} \left[D_i * (B_i \times I) + N_i\right]}{\sum_i B_i^2\, \sigma_i^{-2}} \tag{15.11}$$

This relation is homogeneous to the sky brightness distribution I: the mosaic is corrected for the primary beams attenuation. In practice, a slightly modified mosaic is computed, in order to avoid noise propagation (it makes no sense to add to the center of a field noise coming from the external, attenuated regions of an adjacent field). For that purpose, the primary beams used to construct the mosaic are truncated to some value, typically 10 to 30% of the maximum. The mosaic is thus defined by:

$$J = \frac{\sum_i \frac{B_i^t}{\sigma_i^2} F_i}{\sum_i \frac{B_i^{t\,2}}{\sigma_i^2}} = \frac{\sum_i B_i^t\, \sigma_i^{-2} \left[D_i * (B_i \times I) + N_i\right]}{\sum_i B_i^{t\,2}\, \sigma_i^{-2}} \tag{15.12}$$

where B_i^t denotes the truncated primary beam of the field i. This relation is the measurement equation of a mosaic, connecting the observed quantity J to the sky brightness distribution I (equation 15.1 was the measurement equation of a single-field observation).

Noise distribution

Due to the correction for the primary beams attenuation, the noise distribution in a mosaic is not uniform. From Eq.15.12, it can be written:

$$N = \frac{\sum_i B_i^t\, \sigma_i^{-2}\, N_i}{\sum_i B_i^{t\,2}\, \sigma_i^{-2}} \tag{15.13}$$

Accordingly, the rms depends on the position and is given by:

$$\sigma_J = \frac{\sqrt{\sum_i B_i^{t\,2}\, \sigma_i^{-2}}}{\sum_i B_i^{t\,2}\, \sigma_i^{-2}} = \frac{1}{\sqrt{\sum_i B_i^{t\,2}\, \sigma_i^{-2}}} \tag{15.14}$$

The noise thus strongly increases at the edges of the mosaic (see Fig. 15.1). The non-uniformity of the noise level with the position makes it impossible to use classical CLEAN methods to deconvolve the mosaic: the risk to identify a noise peak as a CLEAN component would be too important. It is thus necessary to identify the CLEAN components on another distribution. For that purpose, the "signal-to-noise" distribution is computed:

$$H = \frac{J}{\sigma_J} = \frac{\sum_i B_i^t\, \sigma_i^{-2}\, F_i}{\sqrt{\sum_i B_i^{t\,2}\, \sigma_i^{-2}}}$$

$$\text{i.e. :} \quad H = \frac{\sum_i B_i^t\, \sigma_i^{-2} \left[D_i * (B_i \times I) + N_i\right]}{\sqrt{\sum_i B_i^{t\,2}\, \sigma_i^{-2}}} \tag{15.15}$$

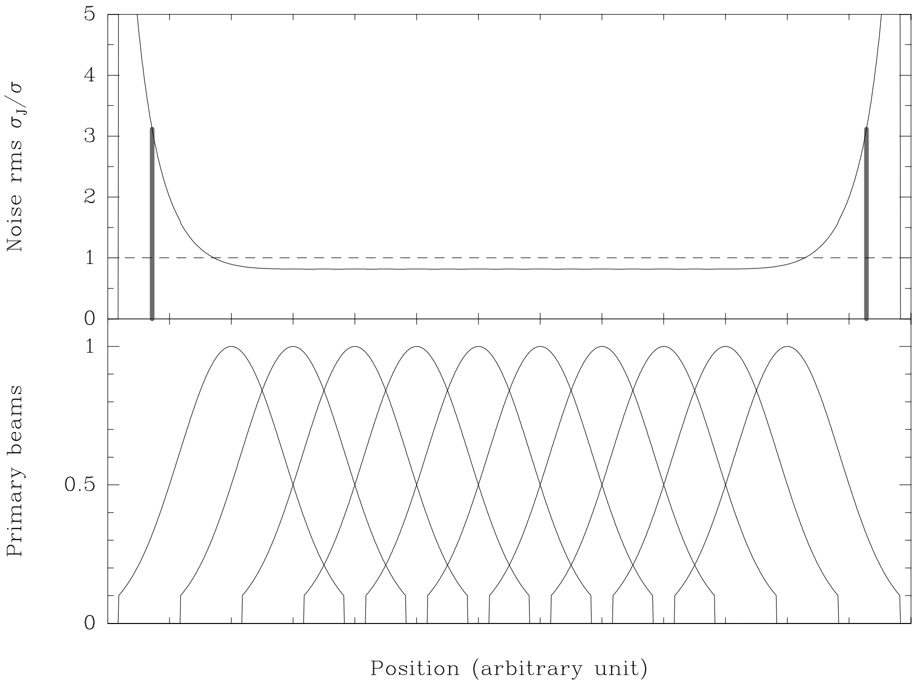

Figure 15.1: One-dimensional mosaic of 10 half-power overlapping fields, with identical noise level σ. (Lower panel:) Normalized primary beams, truncated to $\mathrm{B_{min}} = 0.1$. (Upper panel:) Resulting noise distribution (Eq.15.14). The noise rms in the mosaic is roughly constant, about 20% lower than the noise of each individual field, but strongly increases at the edges. The two thick vertical lines indicate the truncation of the mosaic done by the algorithm at $\sigma_J = \sigma/\sqrt{\mathrm{B_{min}}}$.

Deconvolution algorithm

The main idea of the algorithm is to iteratively find the positions of the Clean components on H, and then to correct the mosaic J. The initial distributions J_0 and H_0 are computed from the observations and the truncated primary beams, according to equations 15.12 and 15.15. The following operations have then to be performed at each iteration k:

1. Find the position (x_k, y_k) of the maximum of H.
2. Find the value j_k of J at the position (x_k, y_k).
3. Remove from J the contribution of a point-like source of intensity γj_k, located at (x_k, y_k) (γ is the loop gain, as in the normal Clean algorithm):

$$J_k = J_{k-1} - \frac{\sum_i B_i^t\, \sigma_i^{-2} \left[D_i * \left[\gamma\, j_k\, B_i(x_k, y_k)\, \delta(x_k, y_k) \right] \right]}{\sum_i {B_i^t}^2\, \sigma_i^{-2}} \tag{15.16}$$

   $\delta(x_k, y_k)$ denotes a Dirac peak located in (x_k, y_k).

4. Do the same for H: remove the contribution of a point-like source of intensity γj_k, located at (x_k, y_k):

$$H_k = H_{k-1} - \frac{\sum_i B_i^t\, \sigma_i^{-2} \left[D_i * \left[\gamma\, j_k\, B_i(x_k, y_k)\, \delta(x_k, y_k) \right] \right]}{\sqrt{\sum_i {B_i^t}^2\, \sigma_i^{-2}}} \tag{15.17}$$

   Note that in the two last relations, the Clean component is multiplied by the true, not truncated primary beam (taken at the (x_k, y_k) position).

After $k_{\max}$ iterations, the mosaic J can therefore be written:

$$J = \frac{\sum_i B_i^t\,\sigma_i^{-2}\left[D_i * \left(B_i \times \left[\sum_{k=1}^{k_{\max}} \gamma\, j_k\, \delta(x_k, y_k)\right]\right)\right]}{\sum_i {B_i^t}^2 \sigma_i^{-2}} + J_{k_{\max}} \tag{15.18}$$

Enough iterations have to be performed to ensure that the residual $H_{k_{\max}}$ is smaller than some user-specified threshold (typically 1 to 3). The comparison between Eqs.15.12 and 15.18 shows that, within the noise, the sum of the CLEAN components can be identified with the sky brightness distribution I. As with the normal CLEAN algorithm, the final clean image is then reconstructed as:

$$M = C * \left[\sum_{k=1}^{k_{\max}} \gamma\, j_k\, \delta(x_k, y_k)\right] + J_{k_{\max}} \tag{15.19}$$

where C is the chosen clean beam. The modified CLEAN algorithms proposed e.g. by [Clark 1980] or [Steer et al 1984] can be similarly adapted to handle mosaics, the main idea being to identify CLEAN components on H and to correct J. Note however that the multi-resolution CLEAN [Wakker & Schwartz 1988] cannot be directly adapted, as it relies on a linear measurement equation, which is not the case for a mosaic.

The MAPPING software

MAPPING is an superset of the GRAPHIC software, which has been developed to allow more sophisticated deconvolutions to be performed. For instance, it allows to choose a support for the deconvolution (clean window) or to monitor the results of the deconvolution after each iteration. Several enhancements of CLEAN (e.g. multi-resolution CLEAN) as well as the `WIPE` algorithm (see lecture by E. Anterrieu) are also available. The deconvolution of a mosaic has to be done with MAPPING. The implemented algorithm assumes that the noise levels in each field are similar (i.e. $\forall i\ \sigma_i = \sigma$), which is a reasonable hypothesis for Plateau de Bure observations. In that case, the equations of the previous paragraph are slightly simplified: J is independent from σ, and H can be written as the ratio H'/σ, where H' is independent from σ and is actually used to localize the CLEAN components.

We refer to the *Mapping Cookbook* for a description of the MAPPING software. In short, to deconvolve mosaics:

- Create a *uv* table for each observed field. Then, run the `UV_MAP` task to compute a dirty map and a dirty beam for each field, with the *same* phase center (variable `UV_SHIFT = YES`).
- The task `MAKE_MOSAIC` is used to combine the fields to construct a dirty mosaic. Two parameters have to be supplied: the width and the truncation level $B_{\min}$ of the primary beams. Three images are produced: the dirty mosaic[3] (yourfile.lmv), all the dirty beams written in the same file (yourfile.beam) and a file describing the positions and sizes of the primary beams (yourfile.lobe). The dirty maps and beams of each individual field are no longer used after this step and can thus be removed if necessary.
- The data have to be loaded into the MAPPING buffers. This is done by the `READ DIRTY yourfile.lmv`, `READ BEAM yourfile.beam`, and `READ PRIMARY yourfile.lobe` commands. The latter automatically switches on the mosaic mode of MAPPING (the prompt is now `MOSAIC>`). From now, the deconvolution commands `HOGBOM`, `CLARK` and `SDI` can be used and will apply the algorithm described above. Use the command `MOSAIC` to switch on or off the mosaic mode if necessary.
- The clean beam of the final image can be specified by the user (variables `MAJOR` and `MINOR`). Otherwise, the clean beam computed from the *first* field will be used. To check if there are differences between the various dirty beams, just use the `FIT` i command, which will indicates the clean beam computed for the ith field.

[3] More precisely, this file contains the non normalized mosaic $\Sigma B_i^t \times F_i$. The proper normalization (see equation 15.12) is further done by the deconvolution procedures.

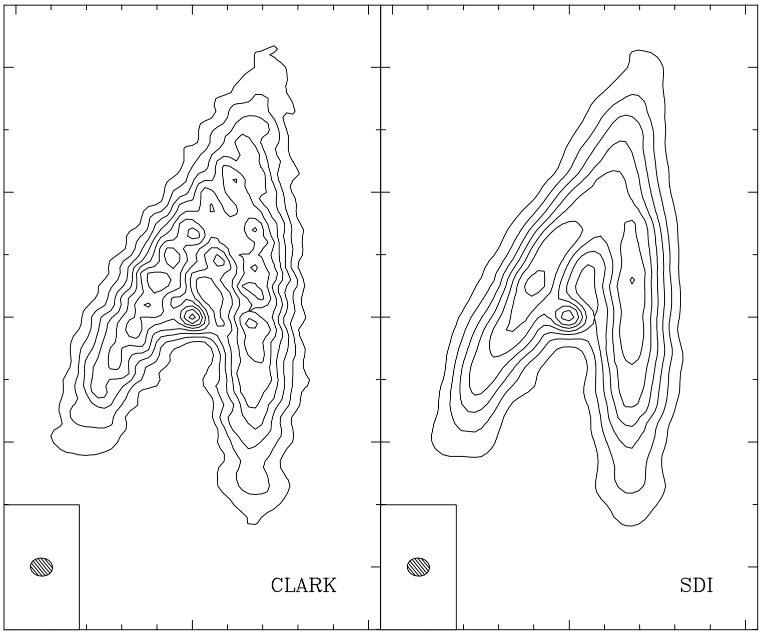

Figure 15.2: Mosaic deconvolved with the `CLARK` or `SDI` algorithms. Deconvolution parameters were identical (with a loop gain 1) and contours are the same in the two images. The formation of stripes does not occur when using the `SDI` algorithm.

- The deconvolution will use the same parameters as a usual CLEAN: support, loop gain, maximal number of iterations, maximal value of the final residual, etc.

- In addition, two other parameters, `SEARCH_W` and `RESTORE_W`, can be supplied. Due to the strong increase of the noise at its edges, the mosaic has to be truncated above some value of σ_J, and these two variables are used to define this truncation level (in terms of $(\sigma_J/\sigma)^{-2}$). More precisely, `SEARCH_W` indicates the limit above which CLEAN components have not to be searched, while `RESTORE_W` indicates the limit above which the clean image is not reconstructed. Default values of these two parameters (both equal to $B_{\min}$) are strongly recommended. The corresponding truncation is shown in Fig. 15.1.

Tests of the method

Several tests of the method described in this paragraph have been performed, either with observations (including the comparison of independent mosaics from the same source) or with simulations. They show that very satisfactory results can be achieved with typical Plateau de Bure observations. Interestingly, `MEM` deconvolution of the same data set (using the task `VTESS` in `AIPS`) seems to give worse results: this is most probably related to the limited uv-coverage obtained with the Plateau de Bure interferometer, as compared to typical VLA observations (`MEM` is known to be vulnerable when there is a relatively small number of visibilities).

15.5 Artifacts and instrumental effects

The behaviour of the mosaicing algorithm towards deconvolution artifacts and/or instrumental effects can be studied by the means of simulations of the whole mosaicing process. The models presented below were computed with several synthetic sky brightness distributions. uv coverage of real observations were used (4–antennas CD configuration of a source of declination $\delta = 68°$). No noise has been added to the simulations shown in the figures, so that pure instrumental effects can directly be seen.

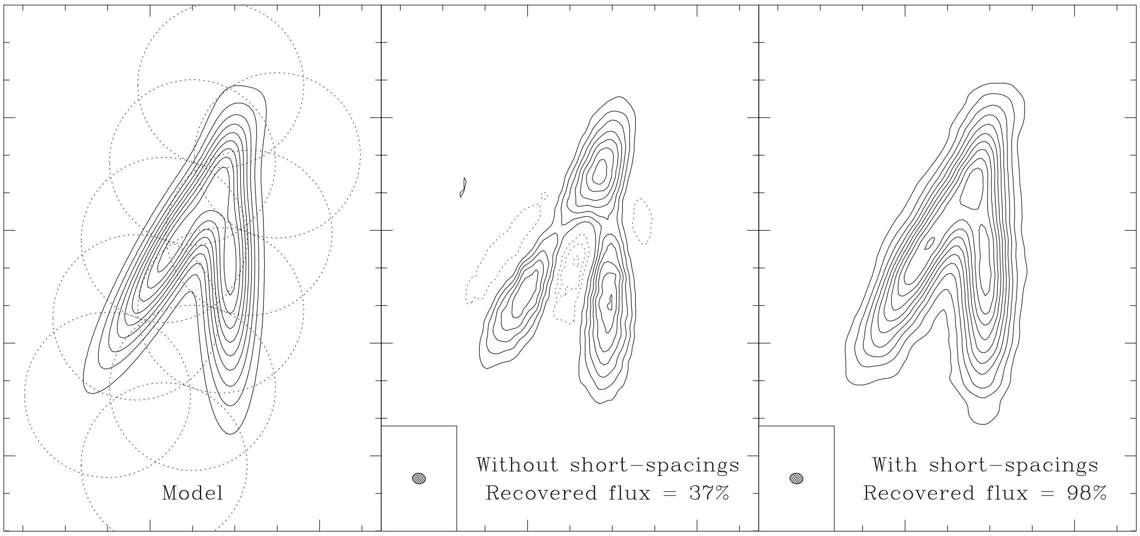

Figure 15.3: (Left:) Initial model of a very extended sky brightness distribution. Dotted circles indicate the primary beams of the simulated observation. (Middle:) Reconstructed mosaic, without the short-spacings information. (Right:) Reconstructed mosaic, with the short-spacings information. The contours are the same in the two simulated observations.

Stripes

A well-known instability of the CLEAN algorithm is the formation of stripes during the deconvolution of extended structures. After the dirty beam has been subtracted from the peak of a broad feature, the negative sidelobes of the beam are showing up as positive peaks. The next iterations of the algorithm will then identify these artificial peaks as CLEAN components. A regular separation between the CLEAN components is thereby introduced and the resulting map shows ripples or stripes. [Steer et al 1984] presented an enhancement of CLEAN (command `SDI` in MAPPING) which prevents such coherent errors: the CLEAN components are identified and removed in groups. As mosaics are precisely observed to map extended sources, the formation of stripes can *a priori* be expected. Indeed, the algorithm described in the previous paragraph presents this instability. Fig. 15.2 shows an example of the formation of such ripples. To make them appear so clearly, an unrealistic loop gain ($\gamma = 1$) was used. But the algorithm of [Steer et al 1984], adapted to the mosaics, does not result in these stripes, even with the same loop gain. It seems thus to be a very efficient solution to get rid of this problem, if it should occur. Note however that more realistic simulations, including noise and deconvolved with normal loop gain, do not show stripes formation. This kind of artifacts seems thus not to play a significant role in the image quality, for the noise and contrast range of typical Plateau de Bure observations. In practice, they are never observed.

Short spacings

The missing short spacings have potentially strong effects on the reconstructed brightness distributions in a mosaic. In each field, the most extended structures are filtered out, which thus introduces a lack of information on an *intermediate* scale as compared to the size of the mosaic. As a consequence, a very extended emission can be split into several pieces, each one having roughly the size of the primary beam. This effect can be very well seen on the simulation presented in Fig. 15.3. Should this problem occur, the only way to get rid of it is to add the short spacings information (deduced typically from single-dish observations) to the data set. Note however that the effects of the missing short-spacings on the reconstructed mosaic strongly depend on the actual *uv* coverage of the observations, as well as on the size and morphology of the source: the artifacts can be small or negligible if the observed emission is confined into reasonably small regions. From this point of view, the example shown in Fig. 15.3 represents the worst case.

In any case, CLEAN is known to be not optimal to deconvolve smooth, extended structures. In order

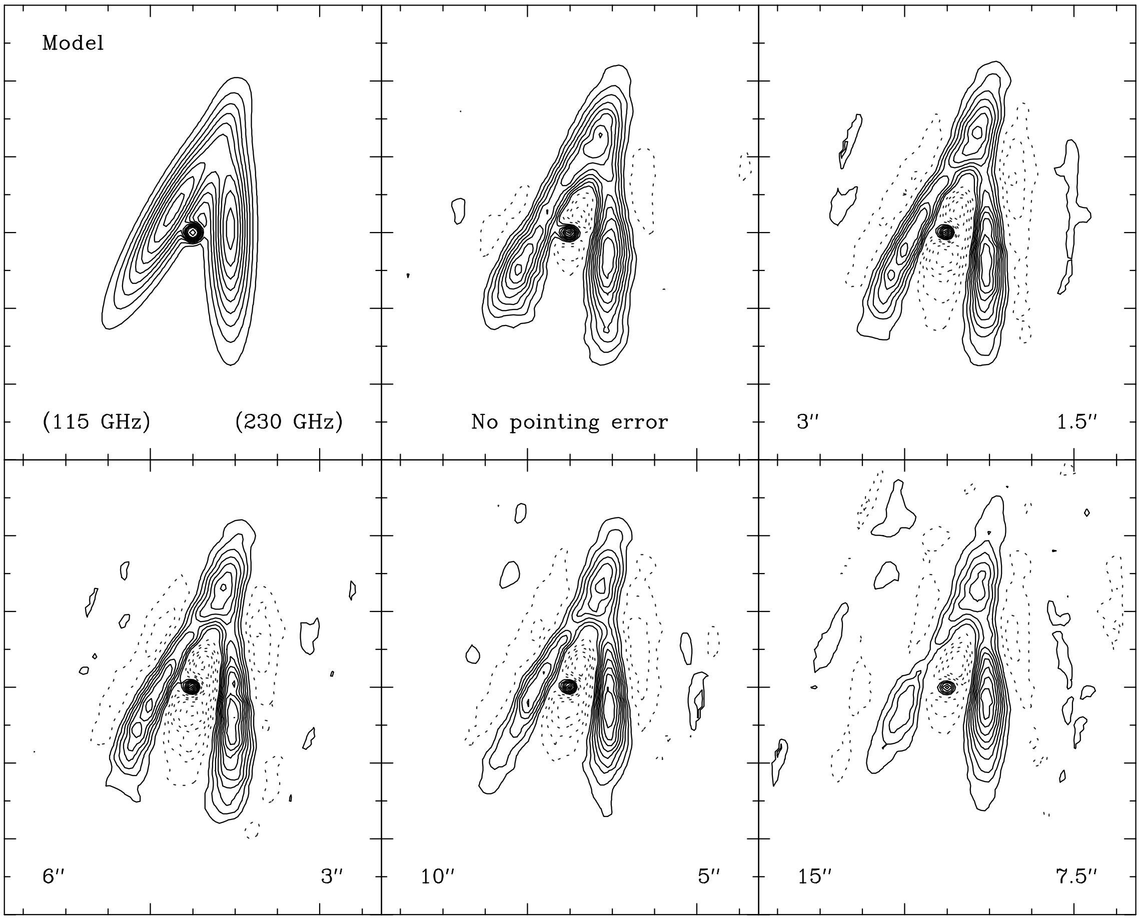

Figure 15.4: Simulations of a 10–fields mosaic observed with the Plateau de Bure interferometer. Each field is affected by a pointing error (see text). The corresponding rms are indicated in the lower left (observations performed at 115 GHz) and lower right (230 GHz) corners of each panel.

to partially alleviate this problem and the effects of the missing short-spacings, [Wakker & Schwartz 1988] proposed an enhanced algorithm, the so-called multi-resolution CLEAN: deconvolutions are performed at low- and high-resolution, and the results are combined to reconstruct an image which then accounts for the extended structures much better than in the case of a classical CLEAN deconvolution. As already quoted before, this algorithm cannot be applied to a mosaic, because it relies on a linear measurement equation. A multi-resolution CLEAN adapted to mosaics has however been developed ([Gueth 1997]) and is currently implemented in MAPPING. This method will not be described here.

Pointing errors

Pointing errors during the observations can of course strongly affect the images obtained by mosaicing. The rms of the pointing errors of the antennas of the Plateau de Bure interferometer is about 3″. By comparison, the primary beam size at 230 GHz is $\sim 22''$ (Table 15.1). The pointing errors are difficult to model precisely: they are different for each antenna, random errors as well as slow drifts occur, the amplitude calibration partially corrects them, etc. A complete simulation should therefore introduce pointing errors during the calculation of each visibility. For typical Plateau de Bure observations, such a detailed modeling is probably not necessary, as the final image quality is dominated by deconvolution artifacts. To get a first guess of the influence of pointing errors, less realistic simulations were thus performed, in which each field is shifted as a whole by a (random) quantity. Such a systematic effect most probably maximizes the distortions introduced in the images. (Note that for a single field, the source would simply be observed at a shifted position in such a simulation. For a mosaic, the artifacts are different, as each individual field has a different, random pointing error. See [Cornwell 1987] for a simplified analysis in terms of visibilities.) Figure 15.4 presents typical reconstructed mosaics for different rms of the pointing errors of the Plateau de Bure antennas. Obviously, the larger the pointing error, the worse the image quality. With a pointing error rms of $3''$, reasonably correct mosaics can be reconstructed even at 230 GHz. Clearly, care to the pointing accuracy has however to be exercised when mosaicing at the highest frequencies.

15.6 Concluding remarks

Mosaic observations are now routinely performed with the Plateau de Bure interferometer, at both λ 3 mm and λ 1.3 mm. Data processing requires a few more operations than normal observations, but does not present any specific difficulties. Reconstruction and deconvolution algorithms are available in the MAPPING software. The number of mosaics actually observed with the Plateau de Bure interferometer regularly increased during the last years. For the last observing period, it amounts about 40% of the mapping projects (the fraction of observing time used for mosaics is much lower, as many time-consuming detection projects are also performed). The number of fields are usually ≤ 6, but can be more important in some cases: the largest mosaic observed up to now (September 1998) has 13 fields.